Proton Affinity and Conformational Integrity of a 24-Atom Triazine Macrocycle across Physiologically Relevant pH

Proton Affinity and Conformational Integrity in a 24-atom Triazine Macrocycle Across Physiologically-relevant pH

Alexander J. Menke,[1] Zachary P. Jacobus,[1] Liam E. Claton,[1] Onofrio Annunziata,[1] Riccardo Capelli,[2] Giovanni M. Pavan[3] and Eric E. Simanek[1,*]

[1] Department of Chemistry & Biochemistry, Texas Christian University, Fort Worth TX 76129 USA

[2] Department of Biosciences, Università degli Studi di Milano, Via Celoria 26, 20133 Milan, Italy

[3] Department of Innovative Technologies, University of Applied Sciences and Arts of Southern Switzerland, Polo Universitario Lugano, 6962 Lugano-Viganello, Switzerland; Department of Applied Science and Technology, Politecnico di Torino, 10129 Torino, Italy

Supporting Information Placeholder

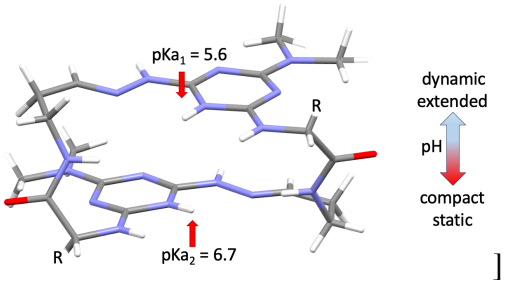

Protonation state influences macrocycle conformation and dynamics.

ABSTRACT: For 24-atom triazine macrocycles, protonation of the heterocycle leads to a rigid, folded structure presenting a network of hydrogen bonds. These molecules derive from dynamic covalent chemistry wherein triazine monomers bearing a protected hydrazine group and acetal tethered by the amino acid dimerize quantitatively in acidic solution. Here, lysine is used and the product is a tetracation. The primary amines of the lysine sidechains do not interfere with quantitative yields of the desired bis(hydrazone) at concentrations of 5–125 mg/mL. Mathematical modeling of data derived from titration experiments of the macrocycle reveals that the pKa values of the protonated triazines are 5.6 and 6.7. Changes in chemical shifts of resonances in the ^{1}H NMR spectra corroborate these values and further support assignment of the protonation sites. The pKa values of the lysine sidechains are consistent with expectation. Upon deprotonation, the macrocycle enjoys greater conformational freedom as evident from the broadening of resonances in the ^{1}H and ^{13}C NMR spectra indicative of dynamic motion on the NMR timescale and the appearance of additional conformations at room temperature. While well-tempered metadynamics suggests only a modest difference in accessible conformational footprints of the protonated and deprotonated macrocycles, the shift in conformation(s) supports the stabilizing role that the protons adopt in the hydrogen-bonded network.

INTRODUCTION

The pharmacokinetic and pharmacodynamic properties of a molecule are affected by ionization state.[1-3] Introducing charge enhances aqueous solubility, mediates protein binding in the vasculature, and influences the nature of intramolecular interactions with a target at the potential expense of membrane permeability. As a function of pH, ionization state will vary with physiological compartment. Accordingly, determining the pKa values for ionizable groups is critical and commonplace. Less common, however, are studies that address the influence of ionization on the conformation of a molecule (outside the realm of molecular machines). While Nature provides numerous examples of proteins that undergo conformational changes as a function of pH, the role that ionization has on the shape of small molecules has been largely unnecessary given traditional, small-molecule drugs. Increasing interest in bioactive macrocycles, however, opens the door to such inquiries.[4-6]

Recently, we reported the use of dynamic covalent chemistry to make macrocycles based on the dimerization of a monomer that presents both acetal and hydrazine groups.[7-12] As ring size increases from 22 to 28 atoms, the shapes of these molecules evolve from stepped to saddle to sheet to crinkled sheet.[7] The

saddle-shaped, 24-atom macrocycles attracted our initial interest for many reasons. First, the yield of the dimerization is often quantitative yielding a twice-protonated product. Second, these protons anchor an intramolecular network of hydrogen bonds. Indeed, this network appears to be responsible for the high yields as it effectively templates ring closure.[8] Third, the sites of protonation are markedly close. Crystallography reveals that the distance between protonated nitrogen atoms is 3.5 Å, placing them almost within van der Waals contact.[9] These observations prompted this series of investigations aimed at the determination of pKa values for these protons and the evaluation of the impact that protonation state has on conformation and dynamics.

To address these questions, a lysine-containing macrocycle, **K-K**, was prepared (Scheme 1). Throughout this report, the charge state is designated with parentheses. The fully protonated macrocycle and neutral molecules are designated **K-K(4+)** and **K-K(0+)**, respectively. Our motivations in choosing lysine as the amino acid were threefold. First, we envisioned that the presence of the ε-amines could limit the generality of the synthetic strategy: the formation of Schiff bases could compete kinetically with the desired, thermodynamically-favored hydrazones.[13] Second, we sought to apply our rules for conformational analysis to this polar target.[9] Third, we hypothesized that the ε-amines would ensure water solubility and facilitate titration over most of the range of physiological pH.

Scheme 1. K-K(4+) with NMR labels (red) and its retrosynthesis. The dotted circles indicate sites of protonation. The hypothesized, templated intermediate is shown with an arrow indicating the site of cyclization. Trifluoroacetate counterions are not shown.

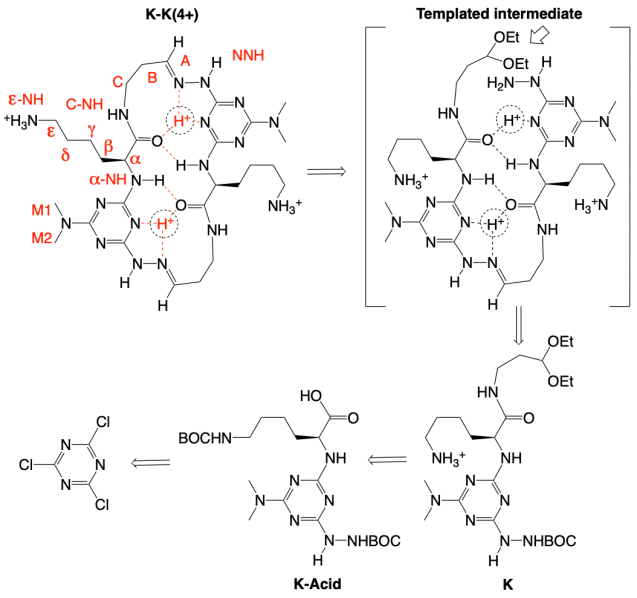

RESULTS AND DISCUSSION

Synthesis. Scheme 1 shows the retrosynthesis of **K-K(4+)**. Synthetic details are available in the supporting information. Briefly, **K-Acid** is the product of the one-pot, stepwise substitution of cyanuric chloride with $BOCNHNH_2$, an ε-protected (BOC) lysine, and finally, dimethylamine. Amidation with an aminoacetal yields monomer **K**. Dimerization to **K-K(4+)** is facilitated with acid and likely proceeds through the templated intermediate (bracketed). The stereochemistry shown derives from the reagent, L-lysine. While the reaction conditions could facilitate epimerization, the observation of a single species either precludes epimerization or would necessitate chiral sorting. This question is the topic of ongoing investigations.

*Selective imine formation leads exclusively to **K-K(4+)**.* Macrocycle **K-K(4+)** is the product of dynamic covalent chemistry. Incorporating an ε-amine into the monomer offers the opportunity for Schiff base formation. While the desired hydrazones are thermodynamically favored,[14] the formation of Schiff bases could lead to undesirable products resulting from kinetic trapping or slowed equilibration to product.[15] Oligomeric or polymeric species represents one potential outcome. Discrete dimeric macrocycles comprising 22- or 23-atom rings (arising from condensation of the acetal with the ε-amine) constitute another. We have shown that 22- and 23-member rings are accessible and not thermodynamically forbidden,[7] although the impact that ring strain could have on sorting has not been explored in this system.[16]

Satisfyingly, the slow evaporation of a 1:1 solution of dichloromethane:trifluoroacetic acid of **K** yields **K-K(4+)** exclusively over a range of concentrations (5 mg/mL to 125 mg/mL of **K**). Purification is not required. The data reported derive from dissolution of the residue in the solvents of interest. Others have reported similar high yields with macrocycles comprising hydrazones.[17] However, and oftentimes, macrocycles derived from dynamic covalent chemistry exist as a mixture of species.

***K-K(4+)** adopts a preferred conformation.* Figure 1 shows the ^{1}H NMR spectra of **K-K(4+)**, monomer **K**, and **K-Acid**. The spectra of **K** and **K-Acid** are markedly different from **K-K(4+)**. Spectral complexity in the two intermediates derives from the existence of rotational isomers (rotamers) arising from hindered rotation about the triazine-N bond. The barrier to rotation for neutral triazines has been calculated and computed to range from 15-18 kcal/mol making these isomers discernable on the NMR timescale.[18,19]

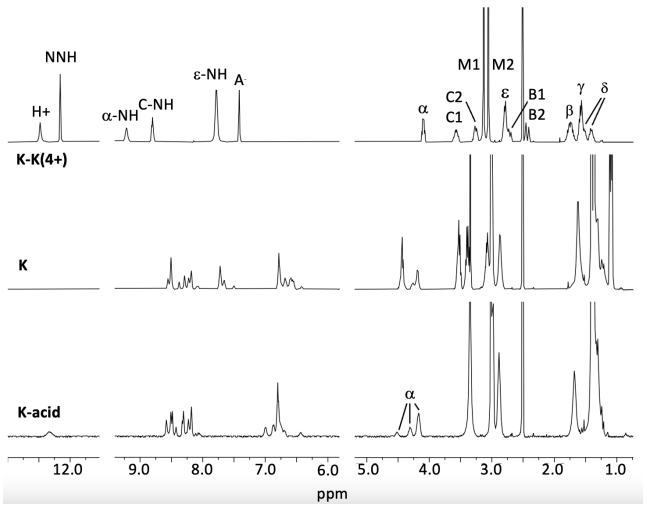

Figure 1. The 400 MHz NMR spectra of protonated K-K, K and K-Acid in DMSO-d_6.

Of the four possible rotamers, three are apparent in the NMR spectrum of **K-Acid** as evident by the resonances for the α proton. The NH region of the spectrum shows similar complexity. The spectrum of monomer **K** also reveals multiple isomers. In contrast, the number of resonances observed for **K-K(4+)** requires that both subunits of adopt identical rotamer conformations. The exchangeable NH protons and H^+ appear far

downfield consistent with hydrogen bonding. All resonances (including H^+ and ε-NH_3^+) integrate for the expected number of protons.

Assigning solution-structure rests on five criteria. We recently described a rapid procedure for determining the solution structure of these macrocycles.[9] The strategy rests on establishing 1) the geometry of the hydrazone, 2) evidence for folding, 3) the site of protonation, 4) the rotamer adopted, and 5) the geometry of the amide.

*An E-hydrazone and folded shape for **K-K(4+)**.* ROESY experiments confirm hydrazone geometry and a folded shape for **K-K(4+)**. The (*E*)-hydrazone is confirmed by rOes between A and NNH. The folded conformation is conveyed by ROESY correlations between A and the methyl groups, M1 and M2, as well as between NNH and M1 and M2. The distances between the protons of the hydrazone and those of the methyl groups within a subunit are too great to be observed by ROESY experiments. Thus, the hydrazone group (A) of one subunit must be in proximity to the dimethylamine group(s) (M1 & M2) of the other subunit to justify the correlation and intensity. These data are consistent with crystral structures reported for related macrocycles comprising valine and glycine, **V-V(2+)** and **G-G(2+)** respectively (Figure 2). Here, morpholine appears in place of dimethylamine, as the former yielded diffraction-quality crystals.

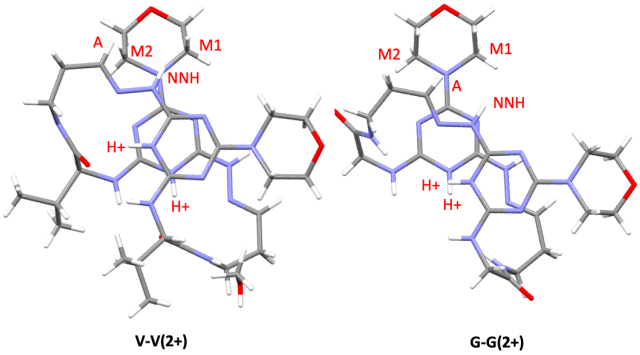

Figure 2. The crystal structures of V-V(2+) and G-G(2+) with H^+ and protons implicated in critical rOes indicated for folding (A-to-M1&M2) and the E-hydrazone (A-to-NNH).

*The rotamer state and sites of protonation for **K-K(4+)** can be inferred, but not rigorously assigned.* Historically, assigning rotamer state and the site of protonation for these macrocycles has been intimately linked. Crystal structures have corroborated solution assignments with the H^+ sitting in a pocket created by the triazine and hydrazone with participation from a nearby carbonyl. This pocket is indicated as a dotted circle in Scheme 1.

For **K-K(4+)**, however, rOes between H+ and other proximate groups, notably α-NH, are not observed and preclude assignment of both the rotamer state and protonation site. We attribute the lack of rOes to rapid exchange of H+, a hypothesis consistent with the broad resonance and its downfield shift in comparison with other macrocycles.

We currently favor a model wherein the protons remains associated with the triazine and in the electron-rich pockets defined by NNH and the carbonyl. The triazine ring is more basic than exocyclic nitrogens on substituents derived from amines. Similarly, computation suggests that the protonated triazine is far more favorable than the protonated hydrazone.[8]

Alternatively, the hydrazone could adopt a different rotamer state that excludes it from contributing to the pocket. Protonation with intimately associated trifluoroacetate counterions could occur. Both models are supported by the downfield shifts of H^+ (more TFA-like) and α-NH (consistent with a stronger hydrogen bond to the carbonyl).

Consistent with chemical intuition, the ^{1}H NMR spectrum of **K-K(4+)** unambiguously assigns two protons to the ε-amine: the resonance integrates for 6H.

Chemical shifts in the ^{1}H NMR suggest a structure similar to other macrocycles. Figure 3 shows the fingerprint region of the NMR spectra in DMSO-d_6 of related macrocycles **V-V(2+)**, **G-G(2+)** and **Aib-Aib(2+)** which incorporate valine (sidechain -$CH(CH_3)_2$), glycine (sidechain -H) and aminoisobutyric acid (sidechain gem-dimethyl groups), respectively, instead of lysine. The spectrum of the deprotonated macrocycle, **K-K(0+)** is also shown. In general, this region reflects common structural features. Trends are seen across the series.

The position of NNH (red dots) reports on the role of NNH in stabilization of H^+. For **K-K(4+)** the role is slightly reduced compared with other macrocycles, which we interpret to be a reflection of dynamic exchange of H^+ with solvent. This participation is still significant, however, given the chemical shift of NNH upon deprotonation, **K-K(0+)**.

Accordingly, in **K-K(4+)**, the resonance for the exchanging H^+ (yellow dots) shifts downfield compared with the other protonated macrocycles due to less stabilization from the electron-rich pocket.

Both C-NH (green dots) and α-NH (blue dots) are sensitive to the protonation state of **K-K** in ways that cannot yet be described. We note that the shift in α-NH mirrors that of H^+. The position of C-NH across the protonated macrocycles is similar with the exception of **Aib-Aib(2+)**. Evaluation of the ROESY spectra and crystal structures of these macrocycles reveals no insight.

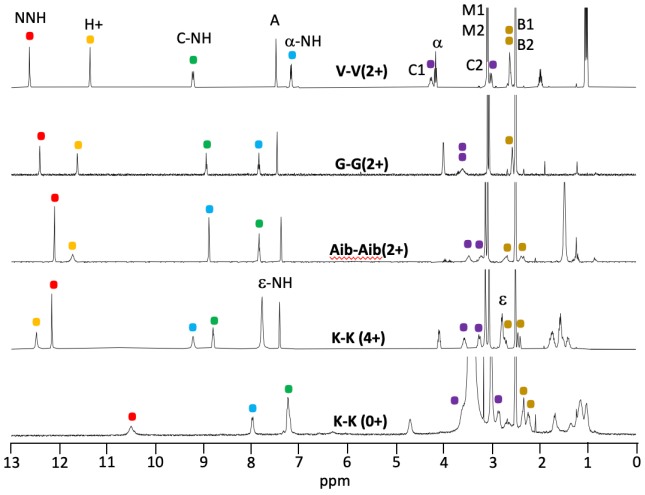

Figure 3. NMR spectra of related macrocycles, the trends observed and the crystal structures of these folded molecules.

Determining pKa values. Evaporation of the TFA:CH_2Cl_2 reaction cocktail provides **K-K(4+)** as a tetracation with four trifluoroacetate counterions as determined by ^{1}H NMR spectroscopy. The pH of a 10 mM aqueous solution of this residue varies from 4.2-4.3. Evaporation of all TFA can be accomplished

under high vacuum. To perform titrations, samples of **K-K(4+)** were dissolved in D_2O in an NMR tube. An electrolyte KCl (150mM) was added to facilitate pD measurements. To ensure complete protonation, 1 μL of trifluoroacetic aid was added to the NMR tube. This sample was titrated with microliter aliquots of 0.10 N NaOH (*aq*). During the titration, ^{1}H NMR spectra were collected periodically. Figure 4 shows the titration curve that results. The values reported in the figures correspond to uncorrected values. A 0.4 unit correction must be applied to the values measured to convert pD to pH.[20,21] Corrected values appear in parantheses in the text.

The pKa values for the protonated triazines can be approximated by inspection, falling between 5 and 7. Mathematical modeling of the titration curve provides these values and those for the sidechains; 5.2 (5.6), 6.3 (6.7), 10.4 (10.8), and 10.6 (11.0), respectively. The former values are consistent with melamine derivatives reported in the literature. Triaminotriazine (melamine) has a pKa of 4.8[22] while methylated derivatives have values ranging from 5.4 to 6.1 as the number of methyl groups increase from 1 to 6.[23] The latter values are consistent with lysine sidechains in peptides and proteins.[24] Details of the modeling can be found in the supporting information. The titration data corroborate structure: protonation of the triazine rings occurs and the sites of protonation communicate with each other (as the pKa values are not equivalent).

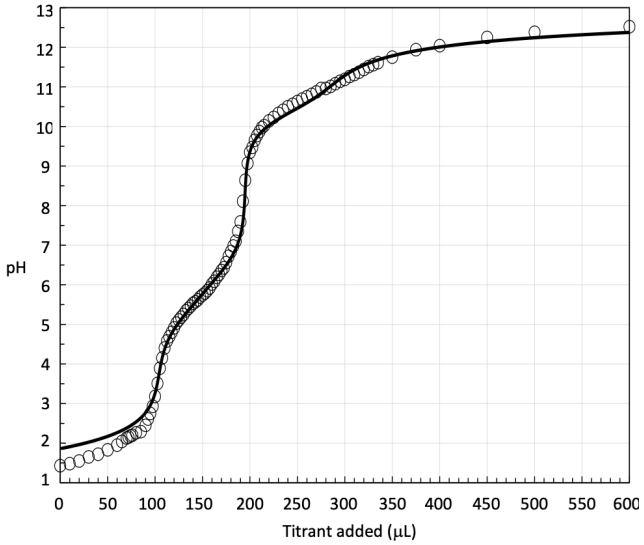

Figure 4. The uncorrected pH titration curve data (circles) and mathematical fit (line).

Figure 5 shows the ^{1}H NMR spectra obtained during the titration. The pH-dependent shifts corroborate structure. Shifts for resonances engaged with H^+ (C-NH, A, α, B1, C1 and C2) occur between pH values of 5.0 (5.4) and 7.0 (7.4), consistent with triazine deprotonation. Similarly, shifts for the δ and ε resonances occur between pH values of 10 (10.4) and 12.5 (12.9) consistent with protonation of the sidechain.

Impact of protonation on conformation. Across the solvents surveyed (CD_3CN, MeOD-d_4, DMSO-d_6, D_2O (pH 2) these rOes are observed, **K-K(4+)** adopts a folded conformation based on the rOes observed (*vide supra*). Upon deprotonation, the rOe for the E-hydrazone is preserved. However, the rOe indicative of a folded conformation is reduced or absent depending on conditions, behavior consistent with extended conformations. At pH 8.0 in D_2O, the rOe is significantly reduced suggesting that **K-K(2+)** samples both folded and extended con-

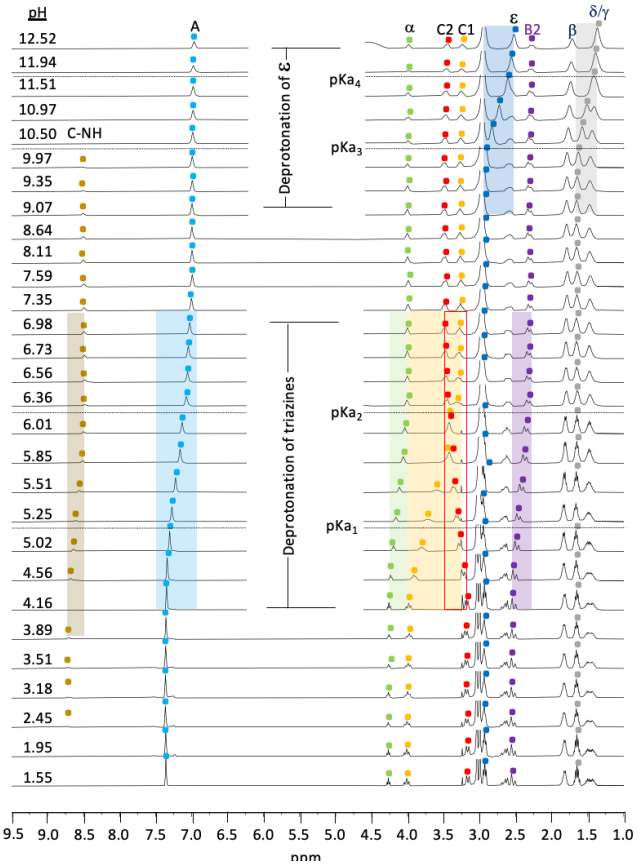

Figure 5. The 400 MHz ^{1}H NMR spectra of K-K in D_2O at different uncorrected values of pH corroborate titration data. Shifts are highlighted with colored dots.

formations. In DMSO-d_6 with Na_2CO_3 added, the rOe is absent suggesting that **K-K(0+)** adopts an extended conformation. Both the ^{1}H and ^{13}C spectra broaden, the latter becoming resolved only upon heating. To evaluate this hypothesis, Well-tempered metadynamics simulations were conducted.

Well-tempered metadynamics suggests similar conformational footprints. We performed well-tempered metadynamics simulations for **K-K(4+)** and **K-K(2+)** with explicit water molecules, the latter more relevant to physiological conditions than the neutral molecule.[25] Two distances comprehensively describe all the possible conformations of these macrocycles (and appear as the axes in Figure 6). These distances separate *i)* proton-bearing nitrogens of the triazines (N-N distance) and *ii)* the *β*-carbons of the lysine residues (*β–β* distance). Both simulations ran 500 ns using GROMACS 2021[26] patched with PLUMED 2.7.[27]

The free energy surfaces (FES) for both **K-K(4+)** and **K-K(2+)** are similar, showing large crescents of low energy, folded conformations (A, A1 & A2) and minima (B) representing the extended conformation. The populations of the minima for **K-K(4+)** and **K-K(2+)** are A (80%) and A1 & A2 (83%), respectively.

Representative structures were extracted from each well. In general, structures obtained from the lower halves of the FES are folded. Moving from left to right corresponds to shifting the π–stacking between subunits from triazine-on-triazine to triazine-on-hydrazone. Structures obtained from the top halves of

the FES are extended. Moving from left to right corresponds to shifting from more compact to fully extended structures.

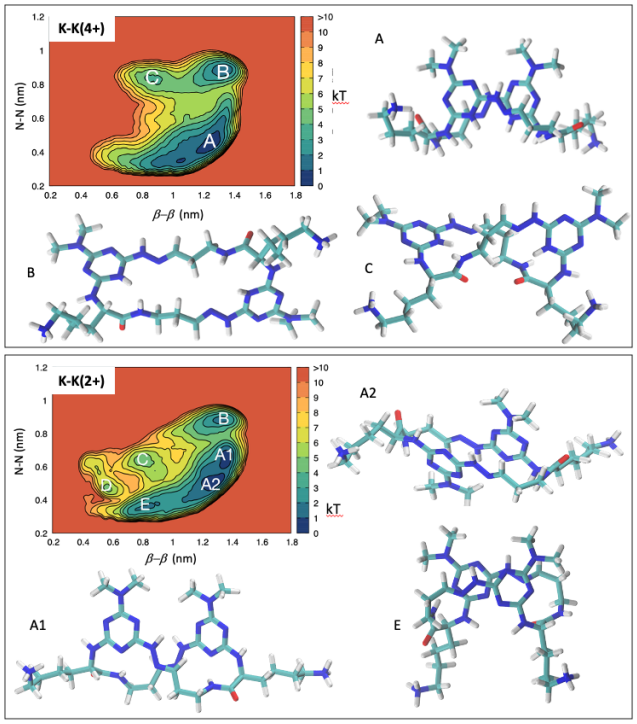

Figure 6. FES of the protonated and deprotonated surfaces with representative structures.

Impact of protonation on dynamic behavior. The sharp NMR spectra and network of rOes observed for **K-K(4+)** are consistent with a structure that is largely static, adopting a preferred folded conformation wherein the carbonyl groups engage in hydrogen bonding with H^+. Orienting carbonyl groups toward protonated heterocycles has been observed in other systems.[28-30]

Consistent with increased motion and multiple conformations upon deprotonation, the ^{1}H NMR spectrum of **K-K(0+)** shows multiple broad resonances that sharpen and/or disappear on heating. Increasing temperature has no such effect on **K-K(4+)**. Acquisitions of ^{13}C NMR for **K-K(4+)** are accomplished quickly, while those of **K-K(0+)** require extended periods of time, consistent with sampling multiple conformations. The coalescence of M1 and M2 are consistent with more dynamic behavior locally in **K-K(0+)**. Most interesting, the FES reveals two compact domains, A1 and A2. Minima A1 is similar to the compact folded structure, but adopts a different rotamer state. Minima A2 is differs both in rotamer state (from A1 and A) as well as the relative orientation of the triazines, head-to-head. No evidence for either state is seen in the ROESY spectrum, however, leading us to the hypothesis that upon deprotonation, **K-K(0+)** samples many different conformations on the NMR timescale including the extended structure.

CONCLUSION

In conclusion, **K-K** can be described as a responsive macrocycle wherein pH dictates either compact or extended conformations. While hydrogen bonds within macrocycles are known to influence structure, such networks are rarely responsive to pH because they rely on amides.[31] In contrast, the conformation of **K-K** is sensitive to pH, presumably because the hydrogen bond network is anchored by the two acidic protons, H^+.

These studies unambiguously establish that pendant primary amine groups do not interfere with cyclization such that kinetic traps are avoided and the yield for cyclization remains quantitative.

Equally important, we establish that both protonated and deprotonated triazines are physiologically relevant with pKa values hovering near 6. The corrected speciation curve for **K-K** is shown in Figure *7*. While one predicts that **K-K** is too polar to cross membranes across the values of physiological pH (shaded), the results suggest that macrocycles incorporating neutral sidechains (ie **V-V**) will exist at multiple charge states at physiological pH (ie **V-V(2+)** and **V-V(1+)**), and accordingly, should yield suitable partition coefficients.[32]

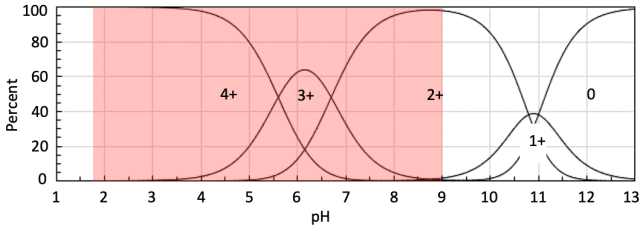

Figure 7. The corrected speciation curve of K-K.

EXPERIMENTAL

Reagents and Solvents. All starting materials were obtained from commercial sources and used without purification including AK Scientific (HOBT), Alfa Aesar (dichloromethane, dimethylforamide, tetrahydrofuran), Cambridge Isotope Laboratories (deuterated NMR solvents) , CHEM-IMPEX (N$^{\varepsilon}$-BOC-L-lysine, trifluoroacetic acid), Cruz (HBTU), Pharmco (ethyl acetate, methanol), Sigma-Aldrich (cyanuric chloride, diisopropylethylamine, diethoxypropylamine).

Instrumentation. All NMR spectra were taken on the 400 MHz Bruker Avance. Solvents were removed via rotary evaporation on a Buchi Rotavapor RII with a Welch Self-Cleaning Dry Vacuum System. The pH of the titration was recorded after stabilization using a VWR SB20 pH meter attached with a Mettler Toledo pH probe.

General Chemistry. Flash chromatography experiments were carried out on silica gel (Silicycle) with a porosity of 60Å, particle size 50–63 μm, surface area 500 –600 m2/g, a bulk density of 0.4 g/mL and a pH range of 6.5 –7.5. Dichloromethane/methanol was used as the eluent for chromatographic purification. Thin-layer chromatography experiments were carried out in sealed chambers and visualized with UV or submersion in ninhydrin (1.5g ninhydrin in 100mL of n-butanol and 3.0mL acetic acid) followed by heating.

Structural assignment. NMR structural assignment relied on COSY, HSQC and ROESY expreiments. Acquisition parameters are reported in the supporting information.

Titrations. Titrations were perfomed in an NMR tube containing **K-K(4+)** (13.1 mg) dissolved in 750 µL D_2O with 1 µL of additional TFA added. Solid KCl (8.4 mg; 150 mM) was added as an electrolyte. An aqueous solution of KHP-standardized NaOH (0.106M) was added using a 25 µL glass syringe in amounts varying from (2.5 – 100 µL) and the pH was recorded stabilization using a VWR SB20 pH meter attached with a Mettler Toledo pH probe. NMR spectra were obtained periodically. The titration curve is shown below (Figure S1). A recorded amount (2.5 – 100 µL) of 0.106 M was added by hand using a 25 µL glass pipette.

Parameterization, Minimization, and Equilibration. The two macrocycles using Avogadro and parameterized the atomistic macrocycle models using the Generalized Amber Force Field (GAFF)[33] with Antechamber.[34] The electrostatic properties were determined via the RESP approach,[35] where single-point charges were derived from HF/(6-31)G* level of theory calculations conducted by Gaussian 16.[36] The macrocycles were then placed within a cubic periodic simulation box filled with TIP3P water[37] (around 6000 molecules). Box charge

was neutralized with trifluoroacetic acetate parameterized with the same protocol used for the macrocycle. To ensure system stability, a two-step minimization process was used: first employing a steepest descent algorithm for 2000 steps, followed by a conjugate gradient algorithm for another 2000 steps. Subsequently, preliminary molecular dynamics (MD) simulations were conducted to raise the system temperature to 298 K, using the velocity-rescale thermostat[38] with a coupling time of 0.2 ps, spanning a total simulation time of 5 ns. Following this, the system was equilibrated in the NPT ensemble under a fixed pressure of 1 bar, achieved by the cell-rescale isotropic barostat,[39] with a coupling time of 1 ps, for an additional 5 ns. Throughout all simulations in this study, a time step of 2 fs was applied, facilitated by LINCS constraints[40] for hydrogen bonds. The simulations were performed using GROMACS 2021[26] patched with PLUMED 2.7.[27]

Well-Tempered Metadynamics Simulations. Tempered Metadynamics (WT-MetaD)[25] simulations lasted 500 ns. These simulations utilized the same MD parameters (as described in the previous section), resulting in the convergence of all systems during this simulation time. Two collective variables (CVs) - distances D1 (between protonated triazine N) and D2 (between β carbons) - were employed as descriptors of macrocycle conformations and conformational changes. For both CVs, we set a sigma of 0.05 nm, a gaussian height of 1.2 kJ/mol, and a bias factor of 25. During the WT-MetaD runs, a Gaussian function was deposited on the landscape every 1 ps. Subsequent to the WT-MetaD simulations, we performed a reweighting procedure using the Tiwary-Parrinello estimator. For the analysis of Free Energy Surfaces (FESs) and population probabilities, the data from the last 400 ns of our simulations was considered.

Synthesis. Details of the synthetic methods and supporting 1D and 2D NMR spectra are available in the SI.

ASSOCIATED CONTENT

Data Availability Statement: The data underlying this study are available in the published article, in its Supporting Information, and openly available at Zenodo, with the DOI 10.5281/zenodo.10379232.

Supporting Information: Available free of charge on the ACS Publications website.

Synthetic, computational, and modelling methods; spectra (PDF)

AUTHOR INFORMATION

Corresponding Author

* e.simanek@tcu.edu

Author Contributions

All authors have given approval to the final version of the manuscript.

ACKNOWLEDGMENT

We thank the Robert A. Welch Foundation (P-0008-19730319) and the NIH (EES R15GM135900). We thank Trevon Jelinek (TCU) for exploratory synthetic efforts and Mr. Davin Haley (R.L. Paschal High School, Fort Worth TX USA) for facilitating the initial efforts of ZPJ.

REFERENCES

1. Mallanack, D. T.; Prankerd, R. J.; Yuriev, E.; Oprea, T. I.; Chalmers, D. K. The Significance of Acid/Base Properties in Drug Discovery. *Chem Soc Rev*. **2013**, *42*, 485–496.

2. Gaohua, L.; Miao, X.; Dou, L. Crosstalk of physiological pH and chemical pKa under the umbrella of physiologically based pharmacokinetic modeling of drug absorption, distribution, metabolism, excretion, and toxicity. *Exp. Opin. Drug Metab. Tox.* **2021**, 10.1080/17425255.2021.1951223

3. Caron, G.; Ermondi, G. Updating molecular properties during early drug discovery. *Drug Disc. Today* **2017**, *22*, 835-840.

4. Ji, X.; Alexander, N. L.; Heinis, C.. Cyclic Peptides for Drug Development. *Angew. Chem. Int. Ed.* **2023**, e202308251.

5. Jimenez, D. G.; Poongavanam, V.; Kihlberg. Macrocycles in Drug Discovery─Learning from the Past for the Future. *J. Med. Chem*. **2023**, *66*, 5377–5396.

6. Villar, E. A.; Beglov, D.; Chennamadhavuni, S.; Porco, J. A.; Kozakov, D.; Vajda, S.; Whitty, A. How Proteins Bind Macrocycles. *Nat. Chem. Biol.* **2014**, *10*, 723– 731.

7. Sharma, V. R; Mehmood, A.; Janesko, B. G.; Simanek, E. E. Efficient syntheses of macrocycles ranging from 22–28 atoms through spontaneous dimerization to yield bis-hydrazones. *RSC Adv.* **2020**, *10*, 3217.

8. Menke, A. J.; Henderson, N. C.; Kouretas, L.; Estenson, A.; Janesko, B. G.; Simanek, E. E. Computational and Experimental Evidence for Templated Macrocyclization: The Role of a Hydrogen Bond Network in the Quantitative Dimerization of 24-Atom Macrocycles. *Molecules*, **2023**, *28*, 1144.

9. Menke, A. J.; Gloor, C. J.; Claton, L. E.; Mekhail, M. A.; Pan, H.; Stewart, M. D.; Green, K. N.; Pavan, G. M.; Capelli, R.; Simanek, E. E. A Model for the Rapid Assessment of Solution Structures for 24-Atom Macrocycles: The Impact of b-Branched Amino Acids on Conformation. *J. Org. Chem.* **2023**, *88*, 2692-2702.

10. Capelli, R.; Menke, A. J.; Pan, H.; Janesko, B. G.; Simanek, E. E.; Pavan, G. M. Well-Tempered Metadynamics Simulations Predict the Structural and Dynamic Properties of a Chiral 24-Atom Macrocycle in Solution. *ACS Omega* **2022**, *7*, 30291.

11. Yepremyan, A.; Mehmood, A.; Asgari, P.; Janesko, B. G.; Simanek, E. E. Synthesis of Macrocycles Derived from Substituted Triazines. *Chembiochem* **2019**, *20*, 241-246.

12. Menke, A. J.; Mellberg, J. M.; Pan, H.; Reibenspies, J. H.; Janesko, B. G.; Simanek E. E. Controlling Swing Rates in Macrocyclic Molecular Mortise Hinges. *Chem. Eur. J.* **2023**, *29*, e202300987.

13. Kulchat, S.; Chaur, M. N.; Lehn, J. M. Kinetic Selectivity and Thermodynamic Features of Competitive Imine Formation in Dynamic Covalent Chemistry. *Chem. Eur. J.* **2017**, *23*, 11108-11118.

14. Yang, Z. Z.; Lehn, J. M. Dynamic Covalent Self-Sorting and Kinetic Switching Processes in Two Cyclic Orders: Macrocycles and Macrobicyclic Cages. *J. Am. Chem. Soc.* **2020**, *142*, 15137-15145.

15. Greenlee, A. J.; Wendell, C. I.; Cencer, M. M.; Laffoon, S. D.; Moore, J. S. Kinetic and Thermodynamic Control in Dynamic Covalent Synthesis. *Trends in Chem.* **2020**, *2*, 1043-1051.

16. Ratjen, L; Vantomme, G and Lehn, JM Strain-Induced Reactivity in the Dynamic Covalent Chemistry of Macrocyclic Imines. *Chem. Eur. J.* **2015**, *21*, 10070-10081.

17. Lin, J, -B.Xu, X. -N.Jiang, X. -K.; Li, Z. -T. Hydrogen Bonding-Directed Multicomponent Dynamic Covalent Assembly of Mono- and Biomacrocycles. Self-Sorting and Macrocycle Exchange. *J. Org. Chem.* **2008**, *73*, 9403–9410.

18. Katritzky, A. R.; Oniciu, D. C.; Ghiviriga, I.; Barcock, R. A. Restricted rotations in 4,6-bis- and 2,4,6-tris-(N,N-dialkylamino)-s-triazines. *J. Chem. Soc. Perk. Trans 2*, **1995**, 785-792.

19. Birkett, H. E. Cherryman, J. C.; Chippendale, A. M.; Hazendonk, P.; Harris, R. K. NMR studies of exchange between triazine rotamers. *J. Molec. Struct.* **2000**, *38*, 504-511.

20. Glasoe, P. K.; Long, F. A. Use Of Glass Electrodes To Measure Acidities In Deuterium Oxide. *J. Phys. Chem.* **1960**, *64*, 188-190.

21. Covington, A. K.; Paabo, M.; Robinson, R. A.; Bates, R. G. Use of the Glass Electrode in Deuterium Oxide and the Relation between the Standardized pD: Scale and the Operationa pH in Heavy Water."Anal. Chem. **1968**, *40*, 700-706.

22. Dixon, J. K.; Woodberry, N. T.; Costa, G. W. The Dissociation Constants of Melamine and Certain of its Compounds *J. Am. Chem. Soc.* **1947**, *69*, 599–600.

23. Gabriel, H.; List, M.; Monkowius, U.; Puchinger, H.; Schwarzinger, C. N-Methylmelamines: Synthesis, Characterization, and Physical Properties. *J. Org. Chem.* **2016**, *81*, 4066−4075

24. Wishart, D. S., Bigam, C. G., Holm, A.; Hodges, R. S.; Sykes, B. D. 1H, 13C and 15N random coil NMR chemical shifts of the

common amino acids. I. Investigations of nearest-neighbor effects. *J. Biomol. NMR* **1995**, *5*, 67–81.

25. Barducci, A.; Bussi, G.; Parrinello, M. Well-Tempered Metadynamics: A Smoothly Converging and Tunable Free-Energy Method. *Phys. Rev. Lett.* **2008**, *100*, 020603.

26. Abraham, J.; Murtola, T.; Schulz, R.; Páll, S.; Smith J. C.; Hess, B.; Lindahl, E. Original software publication GROMACS: High performance molecular simulations through multi-level parallelism from laptops to supercomputers. *SoftwareX* **2015**, *1–2*, 19-25.

27. Tribello, G. A.; Bonomi, M.; Branduardi, D.; Camilloni , C; Bussi, G. PLUMED 2: New feathers for an old bird. *Comp. Phys. Comm.* **2014**, *185*, 604-613.

28. Knipe, P. C.; Thompson, S.; Hamilton, A. D. Acid-mediated topological control in a functionalized foldamer. *Chem. Commun.* **2016**, *52*, 6521-6524.

29. Dolain, C.; Maurizot, V.; Huc, I. Pyridine Protonation-Induced Transition between Two Distinct Helical Conformations of a Synthetic Oligomer via a Linear Intermediate. *Angew. Chem. Int. Ed.* **2003**, *42*, 2737.

30. Takubo, C.; Kimura, S.; Ichinomiya, M.; Hayakawa, A.; Murata, M.; Urushibara, K.; Masu, H.; Katagiri, K.; Kawahata, M.; Kudo, M.; Azumaya, I.; Kagechika, H.; Tanatan, A. Conformational Properties of Aromatic Amides Bearing Imidazole Ring and Acid-Induced Trans−Cis Amide Switching. *J. Org. Chem.* **2022**, ASAP.

31. Liu, Z.J.; Zhou, Y. D.; Yuan, L. H. Hydrogen-bonded aromatic amide macrocycles: synthesis, properties and functions. *Org. Biomol. Chem.* **2022**, *20*, 9023-9051.

32. Patterson-Gardner, C. J.; Pavelich, G. M.; Cannon, A. T.; Menke, A. J.; Simanek, E. E. Adaptation of Empirical Methods to Predict the LogD of Triazine Macrocycles. *ACS Med. Chem. Lett*. **2023**, *14*, 1378–1382.

33. Wang, J., Wolf, R.M., Caldwell, J.W., Kollman, P.A. and Case, D.A. Development and testing of a general amber force field. *J. Comput. Chem.*, **2004**, *25*, 1157-1174.

34. Case, D. A.; Aktulga, H. M.; Belfon, K.; Ben-Shalom, I. Y.; Brozell, S. R.; Cerutti, D. S.; Cheatham III, T. E.; Cisneros, G. A.; Cruzeiro, V. W. D.; Darden, T. A. et al. AMBER 2021. University of California, San Francisco 2021.

35. Bayly, C. I.; Cieplak, P.; Cornell, W.; Kollman, P. A. "A well-behaved electrostatic potential based method using charge restraints for deriving atomic charges: the RESP model." *J. Phys. Chem.* **1993**, *97*, 10269–10280

36. Gaussian 16, Revision B.01, M. J. Frisch, G. W. Trucks, H. B. Schlegel, G. E. Scuseria, M. A. Robb, J. R. Cheeseman, G. Scalmani, V. Barone, G. A. Petersson, H. Nakatsuji, X. Li, M. Caricato, A. V. Marenich, J. Bloino, B. G. Janesko, R. Gomperts, B. Mennucci, H. P. Hratchian, J. V. Ortiz, A. F. Izmaylov, J. L. Sonnenberg, D. Williams-Young, F. Ding, F. Lipparini, F. Egidi, J. Goings, B. Peng, A. Petrone, T. Henderson, D. Ranasinghe, V. G. Zakrzewski, J. Gao, N. Rega, G. Zheng, W. Liang, M. Hada, M. Ehara, K. Toyota, R. Fukuda, J. Hasegawa, M. Ishida, T. Nakajima, Y. Honda, O. Kitao, H. Nakai, T. Vreven, K. Throssell, J. A. Montgomery, Jr., J. E. Peralta, F. Ogliaro, M. J. Bearpark, J. J. Heyd, E. N. Brothers, K. N. Kudin, V. N. Staroverov, T. A. Keith, R. Kobayashi, J. Normand, K. Raghavachari, A. P. Rendell, J. C. Burant, S. S. Iyengar, J. Tomasi, M. Cossi, J. M. Millam, M. Klene, C. Adamo, R. Cammi, J. W. Ochterski, R. L. Martin, K. Morokuma, O. Farkas, J. B. Foresman, and D. J. Fox, Gaussian, Inc., Wallingford CT, 2016.

37. Jorgensen, W. J.; Chandrasekhar, J.; Madura, J.; Impey, R. W.; Klein, M. L.; Comparison of simple potential functions for simulating liquid water. *J. Chem. Phys.* **1983**, *79*, 926–935.

38. Bussi G, Donadio D, Parrinello M. Canonical sampling through velocity rescaling. *J. Chem. Phys.* **2007**, *126*, 14101.

39. Bernetti M, Bussi G. Pressure control using stochastic cell rescaling. *J. Chem. Phys.* **2020**, *153*, 114107.

40. Hess, B., Bekker, H., Berendsen, H.J.C. and Fraaije, J.G.E.M. LINCS: A linear constraint solver for molecular simulations. *J. Comput. Chem.* **1997**, *18*, 1463-1472.